



Universiteit  
Leiden

The Netherlands

## Evolutionary adaptability of $\beta$ -lactamase: a study of inhibitor susceptibility in various model systems

Alen, I. van

### Citation

Alen, I. van. (2023, September 20). *Evolutionary adaptability of  $\beta$ -lactamase: a study of inhibitor susceptibility in various model systems*. Retrieved from <https://hdl.handle.net/1887/3641470>

Version: Publisher's Version


License: [Licence agreement concerning inclusion of doctoral thesis in the Institutional Repository of the University of Leiden](#)

Downloaded from: <https://hdl.handle.net/1887/3641470>

**Note:** To cite this publication please use the final published version (if applicable).

2





# Mutation G132S enhances resistance of *Mycobacterium tuberculosis* $\beta$ - lactamase against sulbactam

Based on the research article:

van Alen, I., Chikunova, A. Safeer, A. A., Ahmad, M. U. D. Perrakis, A., Ubbink, M. (2021) The G132S mutation enhances the resistance of *Mycobacterium tuberculosis*  $\beta$ -lactamase against sulbactam. *Biochemistry* 60 (28), 2236-2245

X-ray crystallography was performed and data were analyzed by A. Chikunova, M. U. D. Ahmad, and A. Perrakis. Laboratory evolution, TSA, NMR spectroscopy, and kinetic experiments were performed in cooperation with A. A. Safeer.

## Abstract

The current rise of antibiotic resistant forms of *Mycobacterium tuberculosis* is a global health threat that calls for new antibiotics. The  $\beta$ -lactamase BlaC of this pathogen prevents the use of  $\beta$ -lactam antibiotics, except in combination with a  $\beta$ -lactamase inhibitor. To understand if exposure to such inhibitors can easily result in resistance, a BlaC evolution experiment was performed, studying the evolutionary adaptability against the inhibitor sulbactam. Several amino acid substitutions in BlaC were shown to confer reduced sensitivity to sulbactam. The G132S mutation causes a reduction in the rate of nitrocefin and ampicillin hydrolysis and simultaneously reduces the sensitivity for sulbactam inhibition. Introduction of the side chain moiety of Ser132 causes the 104-105 peptide bond to assume the cis conformation and the side chain of Ser104 to be rotated toward the sulbactam adduct with which it forms a hydrogen bond not present in the wild-type enzyme. The gatekeeper residue Ile105 also moves. These changes in the entrance of the active site can explain the decreased affinity of G132S BlaC for both substrates and sulbactam. Our results show that BlaC can easily acquire a reduced sensitivity for sulbactam, with a single amino acid mutation, which could hinder the use of combination therapies.



## Introduction

*Mycobacterium tuberculosis* (Mtb) infection ranks among the top 10 causes of death worldwide, with 1.4 million deaths reported in 2019.<sup>128</sup> The treatment of this infection, which currently consists of the administration of four types of antibiotics for a period of six months to two years, is becoming increasingly difficult due to the rise in antibiotic-resistant Mtb strains.<sup>128,129</sup> The gene for BlaC, an Ambler class A  $\beta$ -lactamase,<sup>39,53</sup> is chromosomally encoded in Mtb, rendering treatment of tuberculosis (TB) with  $\beta$ -lactam antibiotics ineffective.<sup>27</sup> However, in light of the current problems with combatting extensively drug-resistant Mtb, this type of antibiotic might provide new opportunities.<sup>119,130–133</sup> There are several Food and Drug Administration-approved compounds available that have the ability to inhibit BlaC, which could constitute an alternative treatment in combination with  $\beta$ -lactam antibiotics.<sup>134,135</sup> Among clinically approved inhibitors for BlaC are clavulanic acid, sulbactam, tazobactam, and avibactam.<sup>89,93,105,136</sup>

The inhibitor for class A  $\beta$ -lactamases that was first discovered and is the best studied is clavulanic acid. Structurally, it is similar to penicillin and inhibits the enzyme by the formation of a covalent bond with Ser70. The adduct can be hydrolyzed slowly at a rate that strongly depends on the ions present in solution.<sup>81</sup> However, various chemical rearrangement reactions can occur in the adduct and multiple trans-enamine adducts have been found using mass spectrometry and X-ray diffraction of crystals. Some adducts are nonhydrolyzable and lead to an inactivated enzyme.<sup>94,95,104</sup>

Sulbactam is a synthetic inhibitor that was developed in 1978 by Wayne E. Barth.<sup>136</sup> It is structurally similar to clavulanic acid and is currently used in the clinic in combination with either ampicillin or cefoperazone.<sup>94,137</sup> It has also shown potential to be used in combination with meropenem.<sup>138</sup> Little is known regarding the mechanism(s) by which sulbactam inhibits BlaC. The inhibitor acts as a substrate that is slowly converted. After inhibition, the enzyme returns to an active state within 30 minutes,<sup>95</sup> which is faster than other first-generation inhibitors do.<sup>81,95,102</sup> Using mass spectroscopy, Hugonnet and colleagues observed the enzyme-inhibitor complex,<sup>95</sup> which has since been crystallized.<sup>104,139</sup> The crystal structure of the trans-enamine adduct formed by BlaC and sulbactam (PDB entry 6H2K<sup>104</sup>) shows differences in the loop region between residues Asp100 and Val108 (Ambler numbering<sup>65</sup>), when compared to resting state enzyme (PDB entry 5OYO<sup>81</sup>), but other parts of the enzyme are minimally affected.

We wondered whether evolution against sulbactam inhibition through mutations in BlaC could easily occur, which could have a negative bearing on the effectiveness of combination therapy. Laboratory evolution yielded mutations A55E, G132S, D172N, and G269S, and their effects on enzyme structure and stability, as well as activity and sulbactam inhibition, are described. Of these mutants, only BlaC G132S exhibits reduced sensitivity for sulbactam inhibition for the

purified enzyme. The crystal structure of the sulbactam adduct shows clear differences from that of wild-type BlaC. The possible mechanism of reduced sulbactam sensitivity is discussed.

## Results

### Laboratory evolution of the Mtb *blaC* gene

A *blaC* gene mutant library was generated using error-prone PCR and cloned into the pUK21 vector. A 42 amino acid *E. coli* twin-arginine translocation (Tat) signal was added at the N-terminus, causing BlaC to be transported to the periplasm of the *E. coli* cells to mimic closely the situation in Mtb.<sup>60,125,140</sup> The resulting strains were screened for resistance against sulbactam in the presence of ampicillin. Plasmids from colonies that showed inhibitor resistance were isolated and sequenced. After  $2 \times 10^6$  clones had been screened, a total of six amino acid substitutions were found in three different *blaC* clones (Table S2.1). The G132S mutation was found as a single mutation in one clone, but also in combination with A55E, D100E, and D179N in another clone. A third clone contained the D172N and G269S mutations. Four of these mutations, A55E, G132S, D17N, and G269S, caused resistance when present in the gene as single amino acid substitutions, albeit to different degrees (Figures 2.1 and S2.1). *E. coli* cells producing wild-type BlaC were able to grow on plates containing  $<8 \mu\text{g mL}^{-1}$  sulbactam in the presence of  $10 \mu\text{g mL}^{-1}$  ampicillin, whereas the cells producing BlaC mutants were able to grow on at least  $10 \mu\text{g mL}^{-1}$  sulbactam. Additive effects with regard to sulbactam resistance were not observed when combining the mutations that originated from the same clone (Figure 2.1).

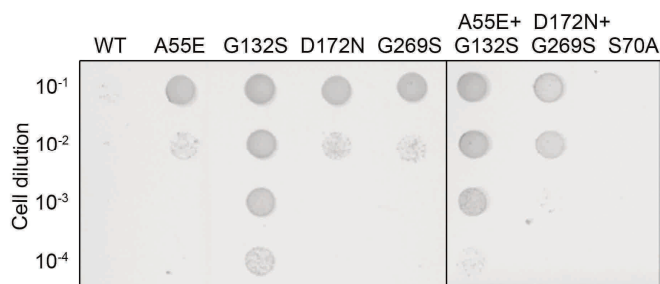


**Figure 2.1.** *In vivo* activity of BlaC mutants in *E. coli*. Cultures of *E. coli* expressing the genes for wild-type BlaC or variants A55E, G132S, D172N, G269S, A55E/G132S, and D172N/G269S were spotted on a plate containing  $10 \mu\text{g mL}^{-1}$  ampicillin and  $8 \mu\text{g mL}^{-1}$  sulbactam. BlaC S70A cannot hydrolyze ampicillin and is used as a negative control. The two panels are pictures of details of a single LB-agar plate placed adjacently for easy comparability of the mutants.

### Protein folding and thermal stability

Overexpression of the BlaC variants, without the signal peptide and with a TEV-cleavable N-terminal His-tag, resulted in soluble, folded enzymes (Figure 2.2a). Thermal shift assays show an increase in melting temperature for BlaC D172N of  $3 \text{ }^\circ\text{C}$  in comparison to that of wild-type BlaC (Figure 2.2b), indicating that the tertiary structure of the mutant is more stable than that of wild-type BlaC. The other mutants showed no change in melting temperature compared to that of the wild-type enzyme (Table S2.2).

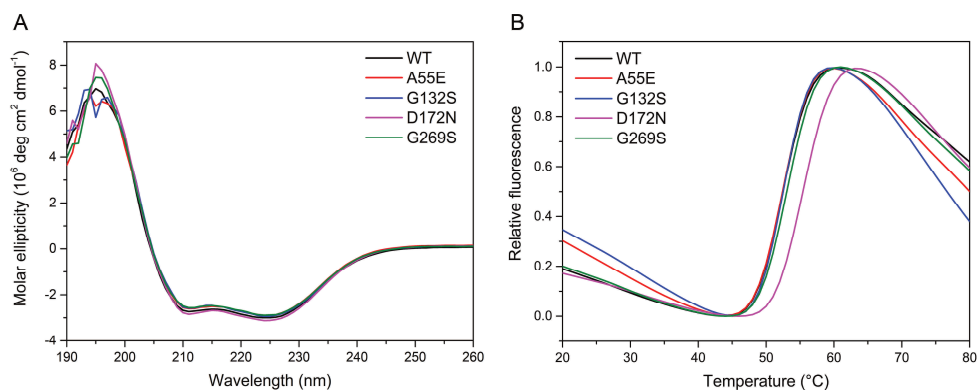


**Figure 2.2.** BlaC mutants are well-folded and stable. (A) Circular dichroism spectra measured for BlaC mutants. (B) Thermal unfolding of BlaC mutants in the presence of SYPRO Orange. Each graph shows the normalized average of six measurements.

### Kinetic parameters

The Michaelis-Menten kinetic parameters for the conversion of nitrocefin and ampicillin show that most mutants exhibit a kinetic profile that is similar to that of wild-type BlaC (Table 2.1). The assays were performed in the presence of BSA (7.6  $\mu\text{M}$ ), which was found to have a stabilizing effect, leading to better reproducibility. The  $k_{\text{cat}}$  and  $K_{\text{M}}$  values for nitrocefin conversion are 2-fold higher than those in the absence of BSA<sup>81</sup> and 10-fold higher than those in the absence of phosphate ions<sup>116</sup>. BlaC G132S performed more poorly than wild-type BlaC in the conversion of nitrocefin, with a 5-fold decrease in  $k_{\text{cat}}/K_{\text{M}}$  (Table 2.1, Figure S2.2). These differences are smaller for the conversion of ampicillin as the  $k_{\text{cat}}/K_{\text{M}}$  is 2-fold lower for BlaC G132S. BlaC D172N can convert nitrocefin with parameters similar to those of the wild-type enzyme yet shows distinct differences for the conversion of ampicillin. There appears to be a decrease in substrate affinity, indicated by a 3-fold higher  $K_{\text{M}}$  compared to the wild type and a 2-fold higher  $k_{\text{cat}}$ .

**Table 2.1.** Kinetic parameters for the hydrolysis of nitrocefin and ampicillin.<sup>a</sup>

BlaC variant	Nitrocefin			Ampicillin		
	$k_{\text{cat}}$ (SD) ( $10^2 \text{ s}^{-1}$ )	$K_{\text{M}}$ (SD) ( $10^2 \mu\text{M}$ )	$k_{\text{cat}}/K_{\text{M}}$ (SD) <sup>b</sup> ( $10^5 \text{ M}^{-1} \text{ s}^{-1}$ )	$k_{\text{cat}}$ (SD) ( $\text{s}^{-1}$ )	$K_{\text{M}}$ (SD) ( $10^2 \mu\text{M}$ )	$k_{\text{cat}}/K_{\text{M}}$ (SD) <sup>b</sup> ( $10^5 \text{ M}^{-1} \text{ s}^{-1}$ )
WT	2.2 (0.2)	5.6 (0.7)	3.9 (0.6)	2.1 (0.1)	1.3 (0.2)	0.17 (0.02)
A55E	1.8 (0.2)	3.9 (0.5)	4.7 (0.7)	2.1 (0.2)	0.89 (0.09)	0.24 (0.03)
G132S	-	-	0.76 (0.07) <sup>c</sup>	1.7 (0.3)	2.7 (1)	0.071 (0.04)
D172N	1.6 (0.2)	4.8 (1)	3.5 (0.9)	4.5 (1)	4.3 (0.7)	0.10 (0.03)
G269S	2.7 (0.4)	5.5 (1)	5.0 (1)	1.7 (0.4)	0.8 (0.2)	0.22 (0.09)

<sup>a</sup> Nitrocefin measurements for BlaC D172N were performed in duplicate, all others in triplicate. The reactions were performed in 100 mM sodium phosphate (pH 6.4) at 25 °C. <sup>b</sup> Errors represent the propagated standard deviation. <sup>c</sup>  $K_{\text{M}} \gg [S]$  and  $k_{\text{cat}}/K_{\text{M}}$  was determined from  $v_0/[S]$ .

To test the inhibition of the mutants by sulbactam *in vitro*, the enzyme, substrate, and inhibitor were mixed at the start of the reaction, performed at 25 °C. The percentage of the converted substrate after reaction for 15 minutes was compared for several concentrations of the inhibitor to the amount of product in the reaction without an inhibitor. Wild-type BlaC could convert 5 % of the nitrocefim in the presence of the highest concentration of sulbactam tested, while BlaC G132S converts 25 % (Figure 2.3). Fitting the product formation curves for wild-type BlaC and BlaC G132S according to model 3 resulted in a 5-fold higher  $K_i$  value for BlaC G132S, indicating a lower affinity of this mutant for sulbactam (Figure 2.4, Table S2.3). The rates of acylation ( $k_7$ ) and hydrolysis ( $k_8$ ) are similar to those of wild-type BlaC.

Curiously, the degree of inhibition of BlaC A55E, BlaC D172N, and BlaC G269S was similar to that of the wild type, even though these variants displayed increased resistance against inhibition *in vivo*. To test whether a difference in temperature was the cause of this result, the experiment was repeated at 37 °C, to match the temperature of the *in vivo* inhibition tests. However, the same results were obtained, indicating that the temperature is not a factor contributing to differences observed between *in vivo* and *in vitro* results (Figure S2.3). We also tested whether the growth of these mutants at higher sulbactam concentrations could be caused by an improved ability to convert ampicillin. No evidence was found for this in either *in vivo* or *in vitro* experiments using single amino acid mutants (Figure S2.4). Interestingly, the combination of mutations D172N and G269S increased the MIC from 60 to >100  $\mu\text{g mL}^{-1}$ , which is higher than for either of the individual mutations.

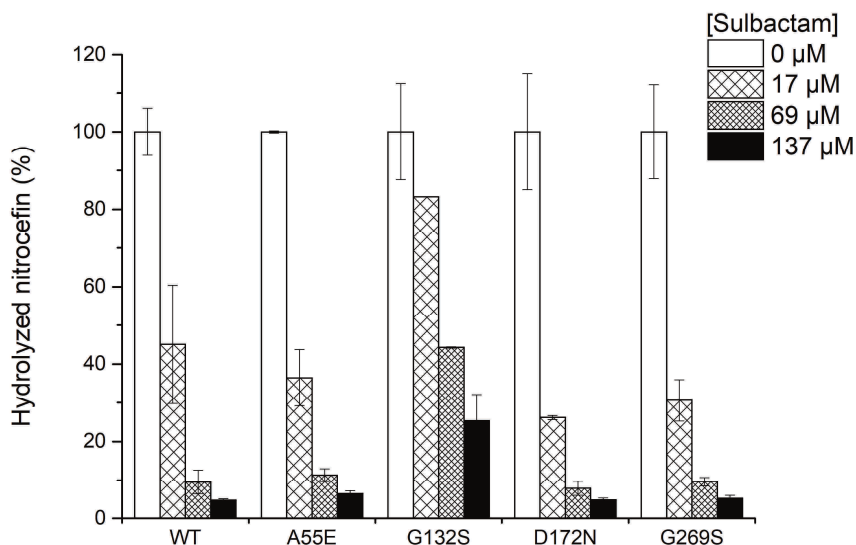


**Figure 2.3.** Hydrolyzed nitrocefim in the absence or presence of sulbactam and BlaC after 15 minutes at 25 °C. Measurements were performed in duplicate in the presence of 125  $\mu\text{M}$  nitrocefim and 2 nM BlaC. The error bars represent one standard deviation.

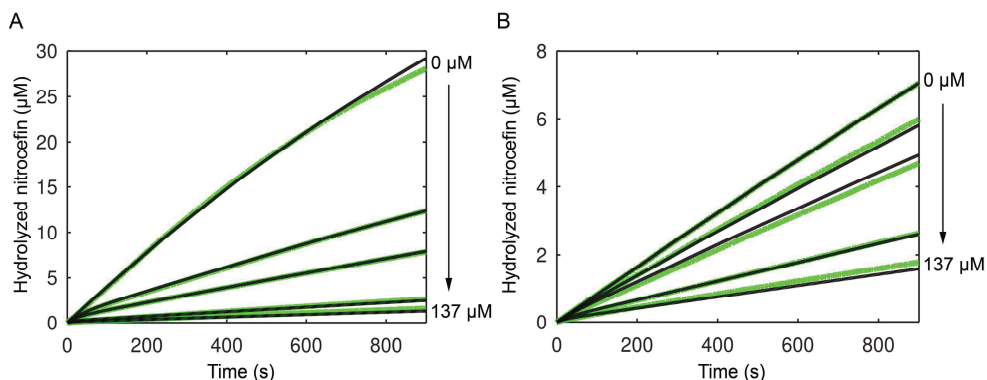


**Figure 2.4.** Effect of sulbactam on the hydrolysis of nitrocefin for (A) wild-type BlaC and (B) BlaC G132S. Green lines represent experimental data, and black lines represent fitted values according to model 2.3. The data were recorded at 25 °C in the presence of 63 µM nitrocefin.

### Structural analysis

To probe the effects of the mutations on the structure of the enzymes,  $^1\text{H}$ - $^{15}\text{N}$  HSQC spectra were recorded (Figures S2.5-S2.8) and averaged chemical shift perturbations (CSP) compared to the spectrum of wild-type BlaC were mapped on a crystal structure of BlaC (PDB entry 5NJ2<sup>81</sup>). BlaC A55E and BlaC G269S show only minor changes in the chemical environment of the backbone amides surrounding the mutation site (Figures S2.9 and S2.10). The D172N mutation causes more prominent changes in the protein (Figure 2.5), both around the site of mutation and in the active site. Average CSPs of  $>0.5$  ppm were observed for the amides of residues in the  $\Omega$ -loop, including Glu166, which is involved in catalysis.<sup>53,80</sup> The data for BlaC G132S show a major influence of the amino acid substitution on the chemical environment of the backbone amides. CSPs are dispersed throughout the entire protein, with major changes in the active site and around the loop that contains the mutation. Gly132 is part of the BlaC SDG loop that is a conserved SDN loop in other class A  $\beta$ -lactamases. This loop has been shown to play a vital role in the inhibition of BlaC by clavulanic acid, and the introduction of asparagine in that position allows BlaC to hydrolyze this inhibitor more efficiently.<sup>116</sup>

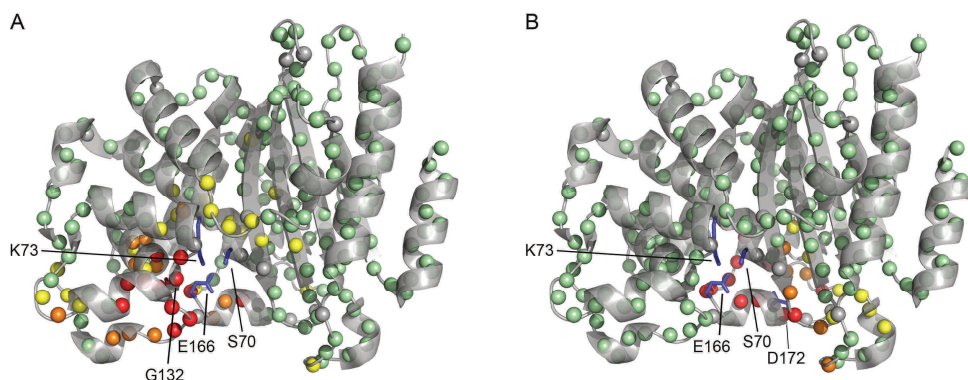


**Figure 2.5.** Average CSPs of (A) BlaC G132S and (B) BlaC D172N plotted on the crystal structure of wild-type BlaC (PDB entry 5NJ2<sup>81</sup>). Backbone amides are represented as spheres and those with CSPs of greater than 0.025, 0.05, and 0.1 ppm are colored yellow, orange, and red, respectively; those with no or small CSPs are colored green, and the ones for which no data are available are colored gray. Mutation sites are indicated and the side chains of active site residues Ser70, Lys73, and Glu166 are represented as sticks.

The crystal structures of BlaC variants A55E, G132S, and D172N were determined to obtain a view of the changes that these mutations cause in the structure. The overall structures are very similar to that of wild-type BlaC with average C $\alpha$  root-mean-square deviations of 0.29, 0.33 and, 0.32 Å, respectively. In the A55E mutant, the  $\gamma$ -carboxy group of Glu55 adds an extra negative charge on the surface of the protein. In the crystal lattice, the  $\gamma$ -carboxyl of Glu55 engages in a hydrogen bond with the symmetry-related side chain of Arg277; notably, the lattice of the A55E mutant deviates from the commonly observed primitive orthorhombic lattice observed for other structures, crystallizing in a closely related but primitive monoclinic lattice, presumably largely owing to this mutated side chain and the new hydrogen bond. The  $\gamma$ -carboxy group also makes three hydrogen bonds involving water molecules. The changes for D172N are less obvious, as the side chain of asparagine occupies the same space as the aspartic acid in the wild-type protein. The carboxamide group of Asn172 forms two highly favorable hydrogen bonding interactions with the side chain carboxyl of Asp179 and the carbonyl of the peptide bond between residues 178 and 179. These favorable interactions not observed for wild-type BlaC stabilize the 171-180 loop and are likely reflected in the increased thermostability of the D172N mutant.

In the G132S mutant, the side chain moiety of Ser104 is forced away by the side chain of Ser132 (Figure 2.6a). The side chain of Ser104 is now turned toward the protein surface, and the carbonyl oxygen of its peptide bond with Ile105 engages in a hydrogen bond with the newly introduced hydroxyl group of Ser132 (Figure 2.6b). This hydrogen bond causes the peptide bond between residues 104 and 105 to assume a *cis* conformation. A similar effect has been described for the G132N mutant<sup>118</sup> and is unique in the available structures of BlaC enzymes. In the structure of the mutant with the trans-enamine adduct of sulbactam, the different positioning of the residues mediated by the G132S mutation as compared to that in wild-type BlaC is maintained, allowing the hydroxyl of Ser104 to form a hydrogen bond with one of the

oxygens of the sulbactam sulfate moiety, not observed in the adduct with wild-type BlaC (PDB entry 6H2K<sup>104</sup>, Figure 2.6c). The interaction with the sulfate moiety through a hydrogen bond with Arg171, observed in the latter structure is also found in the BlaC G132S-adduct complex. This bond freezes the rotational freedom of the sulfate group of the sulbactam adduct in the wild-type enzyme, in a single conformation. The side chain of Ile105 in the structure of the BlaC G132S-adduct complex is not flipped to the side of the active site entrance, as observed for the wild-type BlaC-adduct complex, and is likely pushing away the dimethyl group of the sulbactam adduct. Overall, the *trans*-enamine adduct of sulbactam has more interaction and better packing in BlaC G132S than in wild-type BlaC, which is in apparent contrast with the weakened inhibitory effect in the hydrolysis of substrates. Attempts to elucidate the structure of the *trans*-enamine adduct of sulbactam using mass spectrometry were unsuccessful.

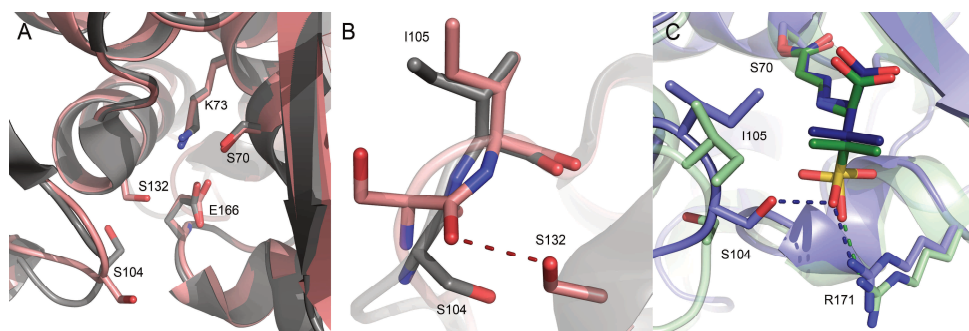


**Figure 2.6.** Crystal structures of BlaC variants. (A) Superposition of the structures of BlaC G132S (salmon, PDB entry 7A71) and the wild type (gray, PDB entry 5OYO<sup>81</sup>) showing the different orientations of S104 and the active site residues in sticks. (B) Overlay of the structures of wild-type BlaC (gray, PDB entry 5OYO<sup>81</sup>) and BlaC G132S (salmon, PDB entry 7A71), showing the *trans* and *cis* peptide bond between residues 104 and 105 in the former and latter. (C) Superposition of the structures with the sulbactam adducts of wild-type BlaC (green, PDB entry 6H2K<sup>104</sup>) and BlaC G132S (blue, PDB entry 7A72).



## Discussion

A laboratory evolution experiment yielded BlaC variants with several amino acid substitutions that cause enhanced *in vivo* resistance against the inhibitor sulbactam. The increased sulbactam resistance *in vivo* is not observed in a nitrocefin activity test *in vitro* for BlaC A55E, D172N, and G269S. Mutants that exhibit reduced affinity or faster hydrolysis of the inhibitor will be picked up in the *in vivo* assay, but selection can also be caused by other factors. The ampicillin concentration was kept low, so *E. coli* clones with mutant enzymes that convert ampicillin at a higher rate than wild-type BlaC would be less hindered by sulbactam, enabling growth on selection plates. The D172N mutant showed such an increased ampicillin conversion rate, though the specificity constant ( $k_{cat}/K_M$ ) was not higher. Differences in the amount of active protein between the mutants, caused by differences in mRNA stability, translation, protein folding, stability, or translocation, could offer another explanation for enhanced resistance against sulbactam *in vivo*. For BlaC D172N, the  $T_m$  is 3 °C higher than that for wild-type BlaC, hinting at increased stability, which we attribute to the increased stability of the  $\Omega$ -loop caused by interactions of Asn172 with residues 178 and 179.

Substitution of Gly with Ser at position 132 decreases the overall catalytic efficiency of the enzyme and at the same time makes it less susceptible to inhibition by sulbactam. Residue 132 is a Gly in BlaC but an Asn in 95% of class A  $\beta$ -lactamases and has been found to be a serine in only two other class A  $\beta$ -lactamases.<sup>141–143</sup> Having a Gly at this position opens up the active site and therefore, purportedly, contributes to the ability of BlaC to convert a broad spectrum of substrates.<sup>116</sup> Ser104 assumes a conformation that resembles the one observed for residue 104 in TEM-1 or SHV-1 (PDB entry 1M40<sup>68</sup> or 1SHV<sup>144</sup>, respectively), in which residue 104 is a Glu or Asp, respectively. The change in the positioning of the loop and the *cis* peptide bond configuration are induced by the side chain at position 132, because the loop would cause steric collisions with Ser104 were it to take the same position as in wild-type BlaC. These changes affect the entire active site as indicated by the CSPs observed for BlaC G132S. The key structural difference appears to be the position of Ile105, previously termed the gatekeeper residue.<sup>125</sup> In the structure of resting state wild-type BlaC, Ile105 partly covers the entrance to the active site, whereas in the adduct with sulbactam, it rotates away, avoiding a steric clash with the adduct.<sup>104</sup> In the resting state structure of BlaC G132S, the side chain of Ile105 has moved 1.6 Å, blocking the active site even more, which is caused by the backbone rearrangement due to the introduction of the Ser at position 132 (Figure 2.6a). In the structure of the mutant with the sulbactam adduct, Ile105 keeps the same position, suggesting that it is more stable in this position in the mutant than in wild-type BlaC. Interestingly, the backbone rearrangement leads to better interactions with the adduct, including a hydrogen bond from Ser104 to the sulfonyl group. This observation seems to be in contrast with the weakened inhibition by sulbactam. However, the structure of sulbactam is very different from that of the adduct. The latter is an elongated molecule without rings, whereas sulbactam has two ring structures, which place the sulfonyl group in a very different position in the active site. The reduced inhibitory effect of sulbactam can be explained by decreased access to Ser70, caused

by the rearrangement of the loop containing Ser104 and Ile105 (Figure 2.7), and is also apparent from the increased  $K_i$  value. Similarly, reduced access of substrate explains the increased  $K_M$  values for nitrocefin and ampicillin (Table 2.2).

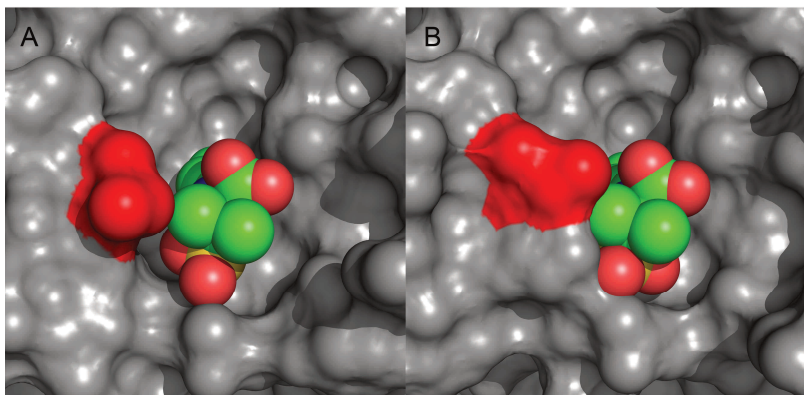


**Figure 2.7.** Surface representation of BlaC variants with the sulbactam adduct. (A) Wild-type BlaC (PDB entry 6H2K<sup>104</sup>) and (B) BlaC G132S (PDB entry 7A72). (B) structures with the sulbactam adduct showing the differences in accessibility of S70 caused by rearrangement in the loop containing residue I105 (red). The sulbactam adduct is shown as spheres.

Soroka and colleagues previously reported that substituting residue 132 with asparagine, thus restoring the SDN motif as present in most  $\beta$ -lactamases, results in an enzyme that can hydrolyze clavulanic acid yet is more sensitive to avibactam.<sup>116,117</sup> Introducing a glycine in class A  $\beta$ -lactamases that have the SDN motif, Bla<sub>Mab</sub>, and KPC-2, improves inhibition by clavulanic acid.<sup>117,145</sup> Interestingly, while we found BlaC G132S is also more sensitive to avibactam, the mutation does not lower resistance to clavulanic acid when compared to that of the wild type (Figure S2.11). Elings *et al.* found that BlaC G132N exists in two forms in solution that are in exchange with a rate of  $\sim 88$  s<sup>-1</sup>.<sup>118</sup> Clearly, the residue at position 132 is critical for the substrate and inhibitor specificity of BlaC. The research question of this work was whether additional resistance against sulbactam could readily be obtained. A single point mutation is already able to increase resistance. However, our study and the work of Soroka *et al.*<sup>116,117</sup> demonstrate that mutation of critical residues often comes at the cost of activity loss or larger sensitivity to other inhibitors, suggesting that judicious choice of inhibitor combinations could slow evolutionary adaptation and resistance of Mtb against a  $\beta$ -lactam/inhibitor treatment. It should be noted though that bacteria of the Mycobacteriaceae family have a cell wall that differs significantly from the cell wall of Enterobacteriaceae, having high lipid and mycolic acid content,<sup>146</sup> so penetration of the compound into the periplasm can differ between these types of bacteria. Our results relate to the inherent catalytic properties of BlaC, but the efficacy of antibiotics and inhibitors is also dependent on the concentration that can be reached at the point of action *in vivo*.

## Materials and methods

The inhibitors sulbactam, avibactam, and clavulanic acid were purchased from Sigma-Aldrich, MedChemExpress, and Matrix Scientific, respectively. It was found that quality can vary between suppliers.

### Screening assays

Laboratory evolution was performed using PCR with DreamTaq DNA Polymerase (Thermo Scientific) under non-optimal conditions (2 mM MgCl<sub>2</sub> and 0.2 mM MnCl<sub>2</sub>) and an unbalanced ratio of nucleotides (0.2 mM dATP, 0.2 mM dGTP, 0.52 mM dCTP, and 0.52 mM dTTP) to increase the error rate during DNA synthesis. The amplified region comprised the *blaC* gene with a twin-arginine translocation-signal peptide sequence (Figure S2.12). Mutations were introduced only in the region of the mature enzyme, not the signal peptide. The product was used for a subsequent standard PCR to increase the quantity of DNA and create a construct with restriction sites. The mutated *blaC* genes were cloned behind the *lac* promoter in pUK21 through restriction and ligation. *E. coli* KA797 cells<sup>147</sup> were transformed with the plasmid library and plated on selective lysogeny broth (LB) agar plates containing 50 µg mL<sup>-1</sup> kanamycin, 10 µg mL<sup>-1</sup> ampicillin, 1 mM IPTG, and 4 µg mL<sup>-1</sup> sulbactam, which is the minimum inhibitory concentration (MIC) for wild-type BlaC in this expression system. Plates were incubated for 16 hours at 37 °C. Colonies were used to inoculate LB containing kanamycin and incubated for 16 hours at 37 °C and 250 rpm before plasmid isolation. To confirm that resistance was the consequence of mutations in the *blaC* gene, plasmids were used to re-transform fresh KA797 cells, which were plated on selective medium. Subsequently, the individual mutations were introduced into the wild-type gene using the QuikChange method (Agilent) and confirmed by DNA sequencing (Table S2.4).

### Inhibitor susceptibility assay

Inhibitor resistance was tested in *E. coli* cells by adding 10 µL of KA797 pUK21-*blaC* liquid cultures with optical densities of 0.3, 0.03, 0.003, and 0.0003 on LB agar plates with various concentrations of the inhibitor and antibiotics. Plates were incubated for 16 hours at 37 °C and imaged using Gel Doc XR+ (Bio-Rad) and ImageLab version 6.0.1 (Bio-Rad).

### Protein production

Protein was produced using *E. coli* BL21 (DE3) pLysS cells transformed with pET28a plasmids containing the *blaC* gene with an N-terminal His-tag and TEV cleavage site (Figure S2.13). Protein was produced and purified as described previously.<sup>81</sup> The size exclusion chromatography step was omitted. Samples for *in vitro* assays contained 100 mM sodium phosphate (pH 6.4).

## Circular dichroism spectroscopy

Protein folding was analyzed using a J-815 circular dichroism (CD) spectrometer (Jasco) with PTC-423S/15 temperature controller (Jasco). Protein samples were diluted to 10  $\mu\text{M}$  and measured in a 1 mm QS High Precision Cell (Hellma Analytics). Spectra were recorded from 260 to 190 nm at 20  $^{\circ}\text{C}$ , and data were collected every 1 nm. Results from five data sets were added to enhance the signal-to-noise ratio.

## Thermal shift assay

Thermal shift assays (TSAs) were performed using a CFX96 Touch Real-Time PCR detection system (Bio-Rad). Protein samples were diluted to a final concentration of 15  $\mu\text{M}$  and mixed with 4x SYPRO Orange Protein Gel Stain (diluted from a 5000x stock as supplied by Sigma-Aldrich) to detect protein unfolding. The temperature (T) was increased from 20 to 80  $^{\circ}\text{C}$  in steps of 1  $^{\circ}\text{C}$ , and samples were incubated for 1 minute at each temperature before detection of the fluorescence signal. Six-fold measurements were performed. Data were analyzed using OriginPro version 9.1 (OriginLab) and fit using equation 2.1:

$$y(T) = A_2 + \frac{(A_1 - A_2)}{\left(1 + e^{\left(\frac{T - T_m}{dT}\right)}\right)} \quad (2.1)$$

where  $T_m$  is the melting temperature in degrees Celsius and  $A_1$  and  $A_2$  are the initial and final values of fluorescence, respectively, and  $dT$  describes the steepness of the change in fluorescence upon unfolding and is thus a measure of the degree of cooperativity.

## Kinetic analysis and *in vitro* inhibition experiments

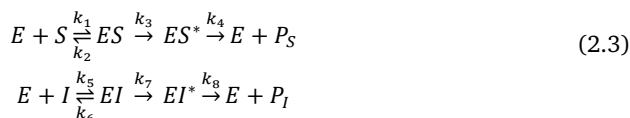
Kinetic parameters were determined for nitrocefin (BioVision) and ampicillin (Serva) as substrates. Measurements were performed in triplicate in a 10 mm QS High Precision Cell (Hellma Analytics), using a PerkinElmer Lambda 800 UV-vis spectrometer thermostated at 25  $^{\circ}\text{C}$ . Nitrocefin hydrolysis by 2 nM BlaC was measured in the presence of 7.6  $\mu\text{M}$  bovine serum albumin (BSA) (Sigma-Aldrich) and various concentrations of substrate, and followed for 3 minutes at 486 nm ( $\epsilon_{486} = 11300 \text{ M}^{-1}\text{cm}^{-1}$ ).<sup>148</sup> Ampicillin conversion by 10 nM BlaC was followed for 4 minutes at 235 nm ( $\epsilon_{235} = 861 \text{ M}^{-1}\text{cm}^{-1}$ ). The kinetic curves were fit, and kinetic parameters were obtained using OriginPro version 9.1 and equation 2.2:

$$v_i = \frac{k_{cat} [E] [S]_0}{K_M + [S]_0} \quad (2.2)$$

where  $v_i$  is the initial slope of the product formation curve as a function of time,  $[S]_0$  is the initial substrate concentration,  $[E]$  is the enzyme concentration and  $k_{cat}$  and  $K_M$  are the standard Michaelis-Menten parameters.

Inhibition assays of BlaC (2 nM in 100 mM sodium phosphate, pH 6.4) were performed in the presence of 125 or 63  $\mu\text{M}$  nitrocefin and 7.6  $\mu\text{M}$  BSA at either 25 or 37  $^{\circ}\text{C}$ . The absorbance at

486 nm ( $\epsilon_{486} = 25700 \text{ M}^{-1}\text{cm}^{-1}$ )<sup>148</sup> was followed for 15 minutes at various inhibitor concentrations. Product formation curves were fit by solving the differential equations derived from model 2.3 using GNU Octave<sup>149</sup> and following the procedure described by Elings *et al.*<sup>81</sup>



where E, S, and I represent BlaC, nitrocefin, and sulbactam, respectively, P<sub>S</sub> and P<sub>I</sub> are the hydrolyzed forms of S and I, respectively, and ES, EI, ES\*, and EI\* represent the non-covalent and covalent intermediates, respectively. The values for  $k_1$ - $k_8$  were obtained by simulation of the reaction curve in the absence of sulbactam and later fixed in the fitting of  $k_5$ - $k_8$  to 0.51  $\mu\text{M}^{-1}\text{s}^{-1}$ , 76.5  $\text{s}^{-1}$ , 380  $\text{s}^{-1}$ , and 120  $\text{s}^{-1}$  for wild-type BlaC and 0.071  $\mu\text{M}^{-1}\text{s}^{-1}$ ; 10.8  $\text{s}^{-1}$ , 380  $\text{s}^{-1}$ , and 120  $\text{s}^{-1}$  for BlaC G132S, respectively.

## NMR experiments

HNCA spectra for BlaC G132S and BlaC D172N and TROSY-HSQC<sup>150,151</sup> spectra for all mutants were recorded at 25 °C using a Bruker AVIII HD 850 MHz spectrometer equipped with a TCI cryoprobe. Samples contained ca. 0.15 mM <sup>15</sup>N BlaC or <sup>13</sup>C,<sup>15</sup>N BlaC samples in 100 mM sodium phosphate (pH 6.4) and 6 % D<sub>2</sub>O. Data were processed with Topspin 4.0.6 (Bruker Biospin) and analyzed using CCPNmr Analysis.<sup>152</sup> Spectra were compared to the TROSY-HSQC and HNCA spectra of wild-type BlaC<sup>81</sup> and average CSPs of backbone amides were calculated using equation 2.4:

$$\Delta\delta = \sqrt{\frac{1}{2} \left( \Delta\omega_1^2 + \left( \frac{\Delta\omega_2}{5} \right)^2 \right)} \quad (2.4)$$

where  $\Delta\omega_1$  and  $\Delta\omega_2$  are the differences in chemical shifts in spectra of the mutant and wild-type enzymes for <sup>1</sup>H and <sup>15</sup>N, respectively. The assignments of the backbone amide resonances have been deposited in the BMRB as entries 50565, 50566, 50563, and 50564 for BlaC A55E, G132S, D172N, and G269S, respectively.

## Crystallization

Crystallization conditions for all BlaC mutants were screened with the sitting-drop vapor diffusion method using the BCS, Morpheus, and JCSG+ (Molecular Dimensions) screens at 20 °C with 100 nL drops with a 1:1 protein:condition ratio.<sup>153</sup> The plates were pipetted by an NT8 Drop Setter (Formulatrix). Protein solutions were used with a concentration of 9 mg mL<sup>-1</sup> for A55E, G132S, and D172N in 20 mM Tris buffer with 100 mM sodium chloride (pH 7.5). Crystals for all mutants grew within a month under various conditions (Table 2.2). A selection of two to five crystals for each mutant was mounted on cryoloops in mother liquor with the addition of 25% glycerol and vitrified in liquid nitrogen for data collection. In addition, four

crystals of G132S BlaC were soaked in corresponding mother liquor with 10 mM sulbactam for 40 minutes. The conditions yielding crystals that were used for structure determination can be found in Table S2.5.

**Table 2.2.** Crystallography conditions.

BlaC variant	Screen condition	Content
A55E	JCSG F7	0.8 M disodium succinate
G132S	JCSG E2	0.1 M sodium cacodylate (pH 6.5), 0.2 M sodium chloride, 2 M ammonium sulfate
G132S with sulbactam	BCS D9	0.1 M sodium cacodylate (pH 5.3), 15 % PEG-SB, 10 % ethylene glycol, 5 % TMate
D172N	Morpheus B2	0.1 M Morpheus buffer 1 (pH 6.5), 30 % EDO_8K, 0.09 M halogens

### X-ray data collection and refinement

X-ray diffraction data were obtained from a single crystal at beamline PXIII of the Swiss Light Source (SLS, Paul Scherrer Institut, Switzerland) for the A55E, G132S, and D172N mutants and at Diamond beamline I04 of the Diamond Light Source (DLS, Oxford, England) for the G132S mutant with sulbactam. The crystallographic diffraction data were processed and integrated using XDS<sup>154</sup> and scaled using Aimless.<sup>155</sup> The structures were determined by molecular replacement with MOLREP<sup>156</sup> from the CCP4 suite<sup>156</sup> using PDB entry 2GDN<sup>53</sup> for A55E, G132S and D172N and PDB entry 6H2K<sup>104</sup> for G132S with sulbactam as a search model. Diffraction data extended to a resolution of 1.4 Å for A55E, G132S, and D172N and to 1.3 Å for G132S with sulbactam. Model building and refinement were performed using Coot and REFMAC.<sup>156</sup> The model was further optimized using the PDB-REDO Web server.<sup>157</sup> A number of residues were modeled in two conformations: Arg128 and Ile186 for A55E; Ser130, Ile186, Asn197, Arg204, Lys219, Met264, and Glu283 for G132S; Arg39, Lys93, Met264, and Tyr272 for G132S with sulbactam; Arg128, Ser130, and Met264 for D172N. For the G132S and G132S with sulbactam, Ser104 was found in the *trans* conformation. MolProbity<sup>158</sup> scores belonged to the 100th percentile for D172N, the 99th percentile for A55E and G132S with sulbactam, and the 96th percentile for G132S. RamaZ<sup>159</sup> scores for A55E, G132S, G132S with sulbactam, and D172N were -1.177, -0.595, -0.889, and -1.019, respectively. All structures had 99 % of their residues in the Ramachandran favored region with two outliers, namely, Cys69 and Arg220. Data collection and refinement statistics can be found in Table S2.5. The structural data have been deposited in the PDB as entries 7A5T, 7A71, 7A72, and 7A5W for BlaC A55E, G132S, G132S with sulbactam, and D172N, respectively.

### Mass spectrometry

Samples of 20 µM BlaC or BlaC G132S in 100 mM sodium phosphate (pH 6.4) were incubated for 5 minutes at 25 °C in the absence or presence of 100 µM sulbactam. The buffer was exchanged to 10 mM ammonium acetate (pH 7) using Micro Bio-Spin 6 columns (Bio-Rad), and a 1 µL sample was loaded onto a nanoEase M/Z protein BEH C4 column (Waters) and

analyzed using a MALDI Synapt G2-Si mass spectrometer (Waters). Data were analyzed using MassLynx MS (Waters).

## Supporting information

**Table S2.1.** Overview of non-synonymous and synonymous mutations found during screenings for resistance against sulbactam.

Clones	Non-synonymous mutations		Synonymous mutations	
	Amino acid	Codon	Amino acid	Codon
1	D172N	GAT > AAT	S130S	AGT > AGC
	G269S	GGT > AGT		
2	A55E	GCA > GAA	R61R	CGT > CGC
	D100E	GAT > GAA	F66F	TTT > TTC
	G132S	GGC > AGC	V194V	GTT > GTA
	D179N	GAT > AAT	D209D	GAT > GAC
3	G132S	GGC > AGC	A51A	GCA > GCT

**Table S2.2.** Melting temperatures of BlaC mutants. Thermal shift measurements were performed with SYPRO orange fluorescent dye and melting curves were fitted to determine the melting temperature. Values represent the average and standard deviation of six measurements.

BlaC variant	T <sub>m</sub> (SD) (°C)
WT	52.5 (0.3)
A55E	52.4 (0.2)
G132S	52.5 (0.2)
D172N	55.5 (0.1)
G269S	53.1 (0.4)

**Table S2.3.** Kinetic parameters for the inactivation of BlaC and BlaC G132S by sulbactam as determined with model 3. K<sub>i</sub> is the ratio k<sub>6</sub>/k<sub>5</sub>. Measurements were performed in duplicate. Errors in brackets represent one standard deviation.

BlaC variant	K <sub>i</sub> (10 <sup>1</sup> μM)	k <sub>7</sub> (10 <sup>-2</sup> s <sup>-1</sup> )	k <sub>8</sub> (10 <sup>-3</sup> s <sup>-1</sup> )
WT	3.4 (0.3) <sup>a</sup>	10 (1)	11.7 (0.3)
G132S	17 (1) <sup>a</sup>	5.95 (0.02)	15.2 (0.4)

<sup>a</sup> Errors represent propagated standard deviation.

**Table S2.4.** List of primers used to introduce mutations in *blaC*.

Mutation	Primers
A55E	CAACCGGCACCACCGAAGCAATTGAATATCGTG CACGATATTCAATTGCTTCGGTGGTGCCGGTTG
G132S	GCAATTCGTTATAGTGATAGCACCGCAGCCAATC GATTGGCTGCGGTGCTATCACTATAACGAATTGC
D172N	GCCTGGTGATGAACGTAATACCACCACACCGCATGC GCATGCGGTGTGGTGGTATTACGTTTCATACCAGGC
G269S	GAGCGATCGTGCCAGTGGTGGCTATGATGCC GGCATCATAGCCACCACTGGCAGCATCGCTC



**Table S2.5.** Data collection and refinement statistics of crystal structures.

	A55E	G132S	G132S + sulbactam	D172N
PDB	7A5T	7A71	7A72	7A5W
Wavelength (Å)	1.000	1.000	0.912	1.000
Resolution (Å)	38.2-1.40 (1.42-1.40)	44.7-1.40 (1.42-1.40)	78.2-1.30 (1.32-1.30)	44.8-1.40 (1.42-1.40)
Space group	P 1 21 1	P 21 21 21	P 21 21 21	P 21 21 21
Unit cell a, b, c (Å)	39.00, 54.36, 53.69	53.30, 54.32, 78.85	53.49, 54.66, 78.20	54.03, 54.47, 78.78
$\beta$	91.94	90.00	90.00	90.00
CC <sub>1/2</sub>	98.5 (75.2)	98.9 (65.4)	99.9 (65.5)	99.7 (77.7)
R <sub>meas</sub> (%)	13.4 (56.8)	16.3 (130.6)	9.3 (140.7)	7.5 (94.7)
$\langle I/\sigma(I) \rangle$	5.2 (1.7)	8.3 (2.6)	11.1 (1.3)	9.3 (1.8)
Completeness (%)	96.9 (94.2)	98.9 (97.4)	98.2 (99.8)	98.0 (98.0)
Multiplicity	2.5	3.7	5.7	3.0
Unique reflections	42718	45293	56098	45377
Atoms protein/ligands/water	2013/59/207	2047/61/201	2034/37/221	2008/29/156
Bfactors protein/ligands/water (Å <sup>2</sup> )	10/22/19	8/25/20	15/24/26	16/28/28
R <sub>work</sub> /R <sub>free</sub> (%)	14.8/17.7	13.0/16.1	15.2/18.9	13.5/17.2
Bond lengths RMSZ/RMSD (Å)	1.056/0.014	1.270/0.016	1.249/0.016	1.236/0.016
Bond angles RMSZ/RMSD (°)	1.085/1.781	1.120/1.837	1.168/1.940	1.155/1.919
Ramachandran plot preferred/outliers	248/2	248/2	259/2	245/2
RamaZ score	-1.177	-0.595	-0.889	-1.019
Clash score	2.42	4.52	1.94	1.48
MolProbity score	1.02	1.23	0.96	0.89

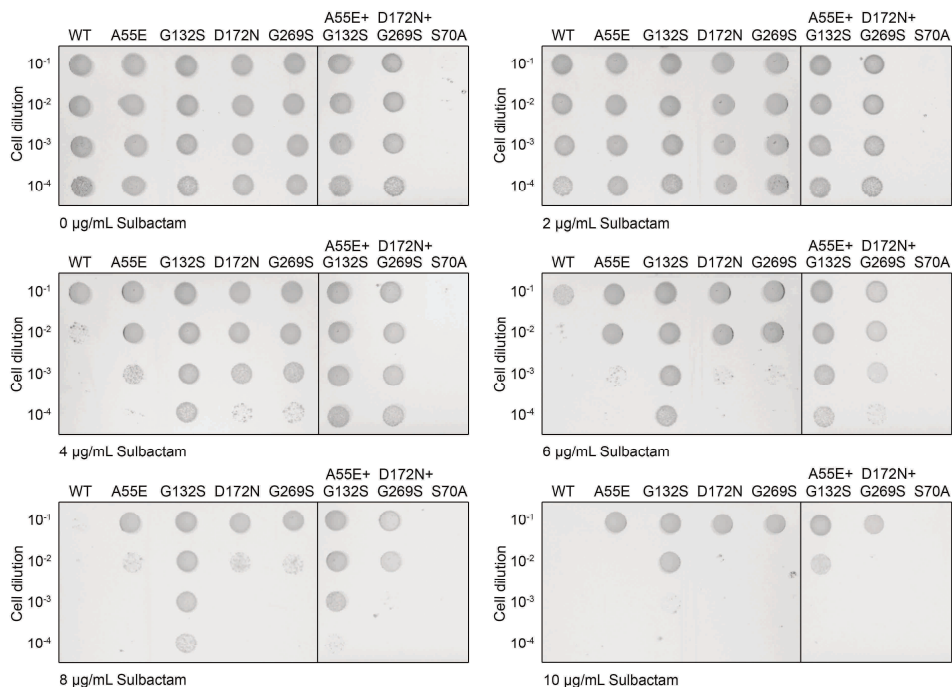


**Figure S2.1.** *In vivo* activity of Mtb BlaC mutants in *E. coli*. *E. coli* cells expressing the genes of wild-type BlaC, and BlaC variants A55E, G132S, D172N, G269S, A55E/G132S, or D172N/G269S were spotted on a plate containing  $10 \mu\text{g mL}^{-1}$  ampicillin and sulbactam. BlaC S70A cannot hydrolyze ampicillin and is used as a negative control. The two panels at each sulbactam concentration originate from the same LB-agar plate.

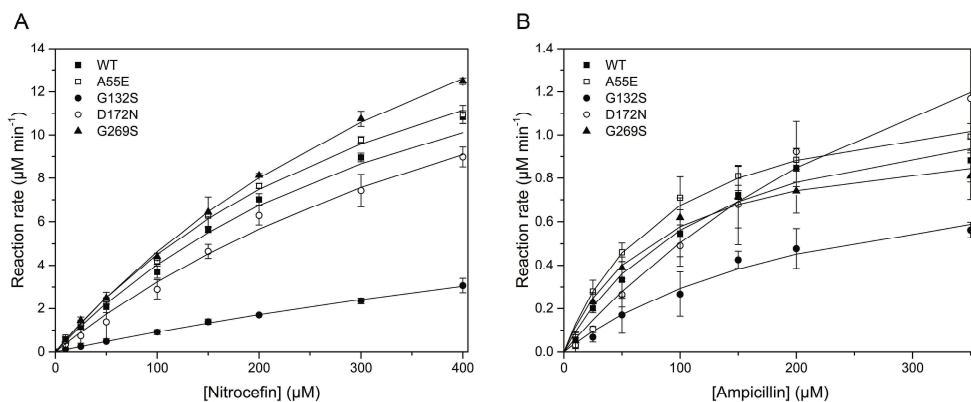


**Figure S2.2.** Michaelis-Menten curves of BlaC mutants for (A) nitrocefin and (B) ampicillin. Experiments were performed at  $25^\circ\text{C}$  in  $100 \text{ mM}$  sodium phosphate ( $\text{pH } 6.4$ ). Error bars represent the standard deviation of three measurements.

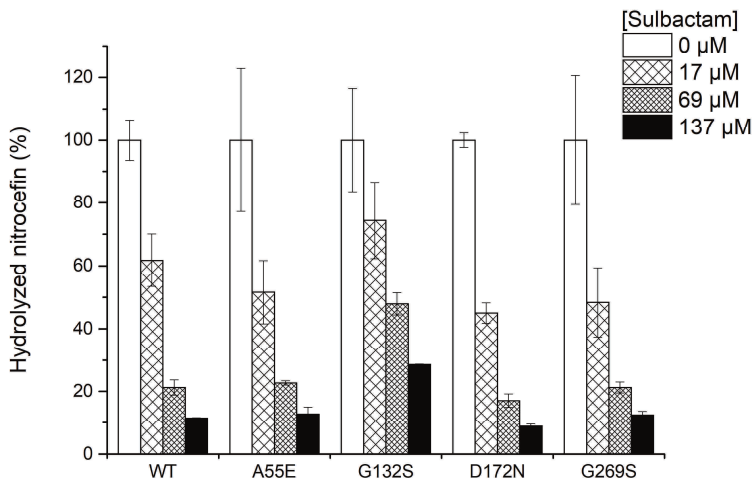


**Figure S2.3.** Hydrolysis of nitrocefim after incubation with sulbactam and BlaC for 15 minutes at 37 °C. Measurements were performed in duplicate. The error bars represent one standard deviation.

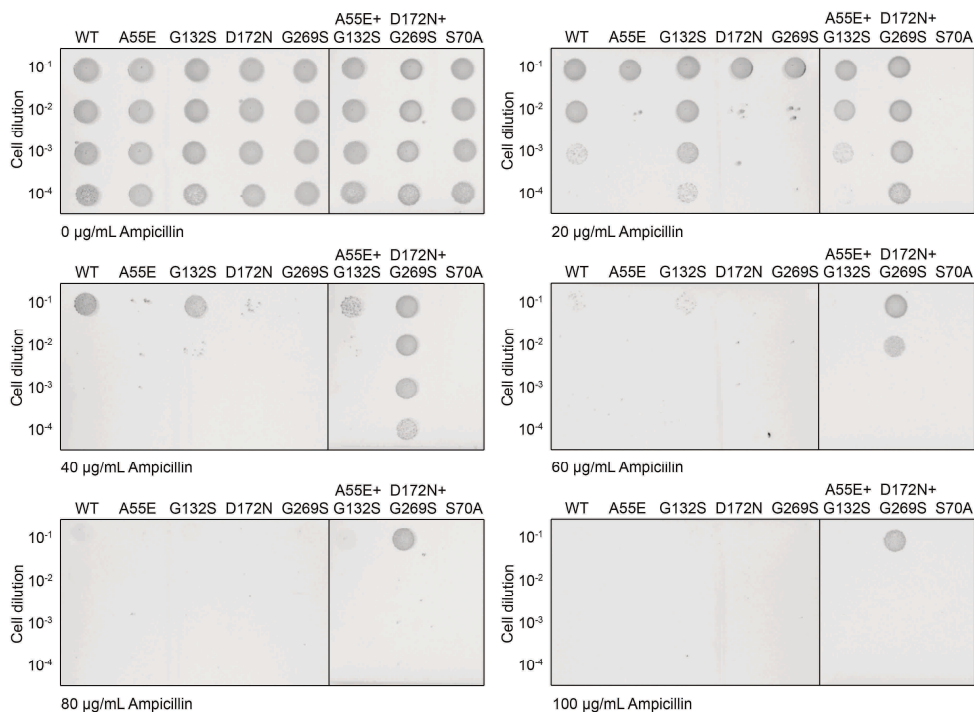


**Figure S2.4.** *In vivo* ampicillin conversion activity of MtB BlaC mutants in *E. coli*. *E. coli* cells expressing the genes of wild-type BlaC, or BlaC variants A55E, G132S, D172N, G269S, A55E/G132S, or D172N/G269S were spotted on a plate containing ampicillin. BlaC S70A cannot hydrolyze ampicillin and is used as a negative control. The two panels at each ampicillin concentration originate from the same LB-agar plate. Note that the combination mutant D172N/G269S has enhanced activity against ampicillin.

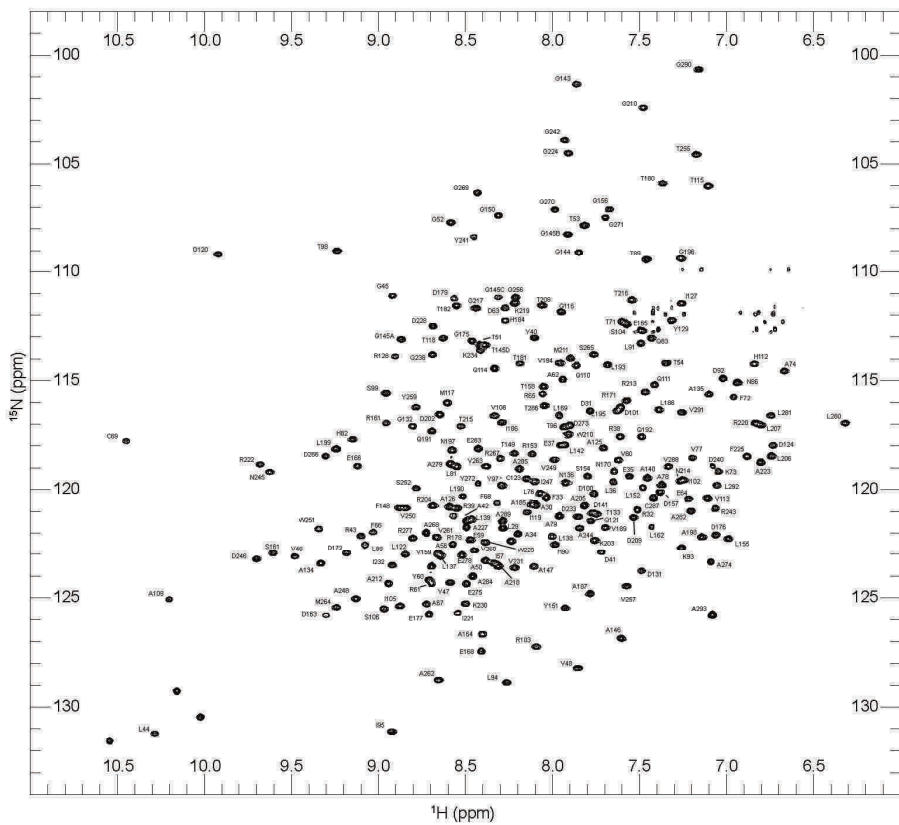


**Figure S2.5.** TROSY-HSQC spectrum of BlaC A55E with residue assignments. Spectrum was obtained at 25 °C using a Bruker AVIII HD 850 MHz spectrometer equipped with a TCI cryoprobe. Sample contained ca. 0.15 mM  $^{15}\text{N}$  BlaC in 100 mM sodium phosphate (pH 6.4) and 6%  $\text{D}_2\text{O}$ . Numbering refers to Ambler numbering.<sup>65</sup> The assignments of the backbone amide resonances have been deposited in the BMRB under entry 50565.

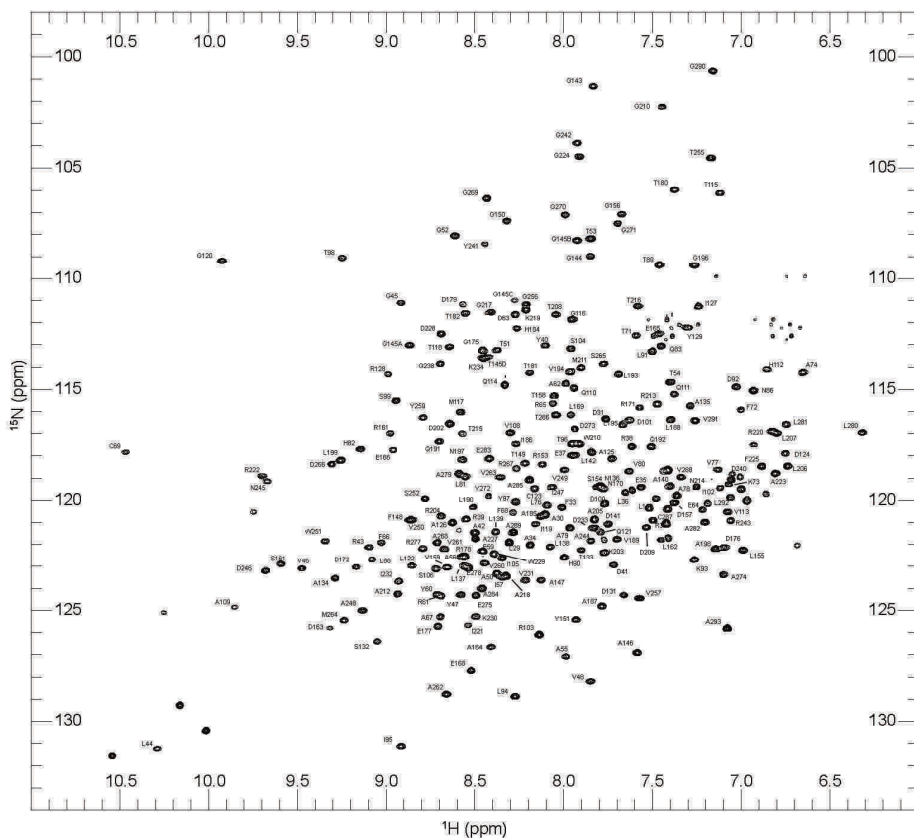


**Figure S2.6.** TROSY-HSQC spectrum of BlaC G132S with residue assignments. Spectrum was obtained at 25 °C using a Bruker AVIII HD 850 MHz spectrometer equipped with a TCI cryoprobe. Sample contained ca. 0.15 mM  $^{15}\text{N}$  BlaC in 100 mM sodium phosphate (pH 6.4) and 6%  $\text{D}_2\text{O}$ . Numbering refers to Ambler numbering.<sup>65</sup> The assignments of the backbone amide resonances have been deposited in the BMRB under entry 50563.

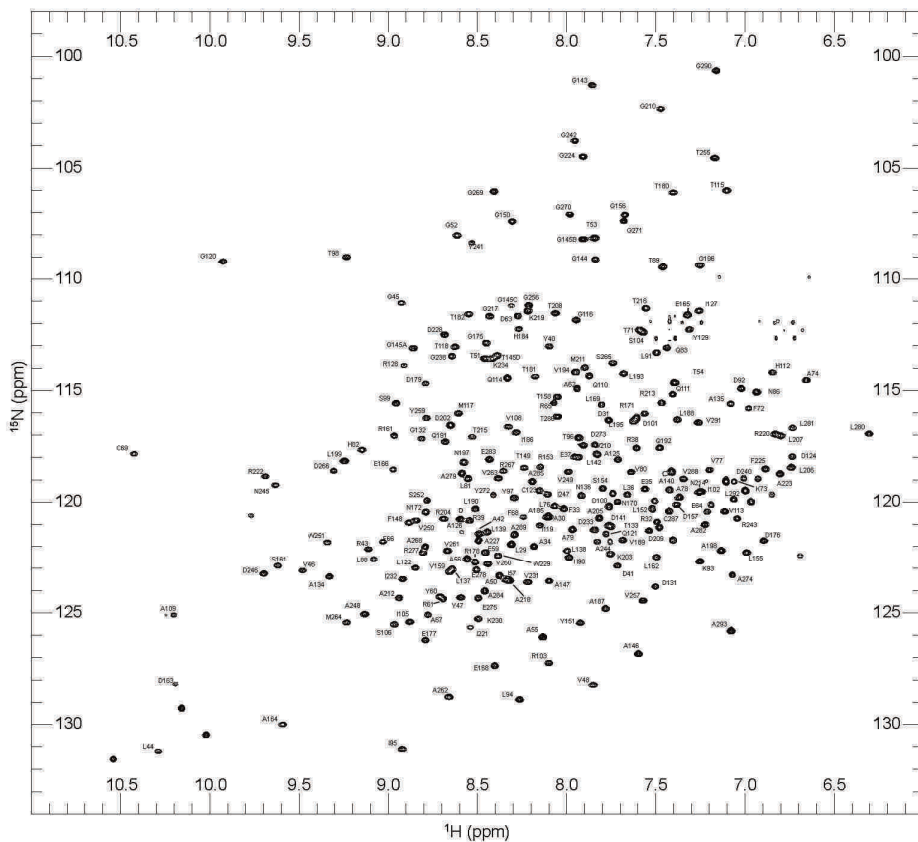


**Figure S2.7.** TROSY-HSQC spectrum of BlaC D172N with residue assignments. Spectrum was obtained at 25 °C using a Bruker AVIII HD 850 MHz spectrometer equipped with a TCI cryoprobe. Sample contained ca. 0.15 mM  $^{15}\text{N}$  BlaC in 100 mM sodium phosphate (pH 6.4) and 6%  $\text{D}_2\text{O}$ . Numbering refers to Ambler numbering.<sup>65</sup> The assignments of the backbone amide resonances have been deposited in the BMRB under entry 50566.

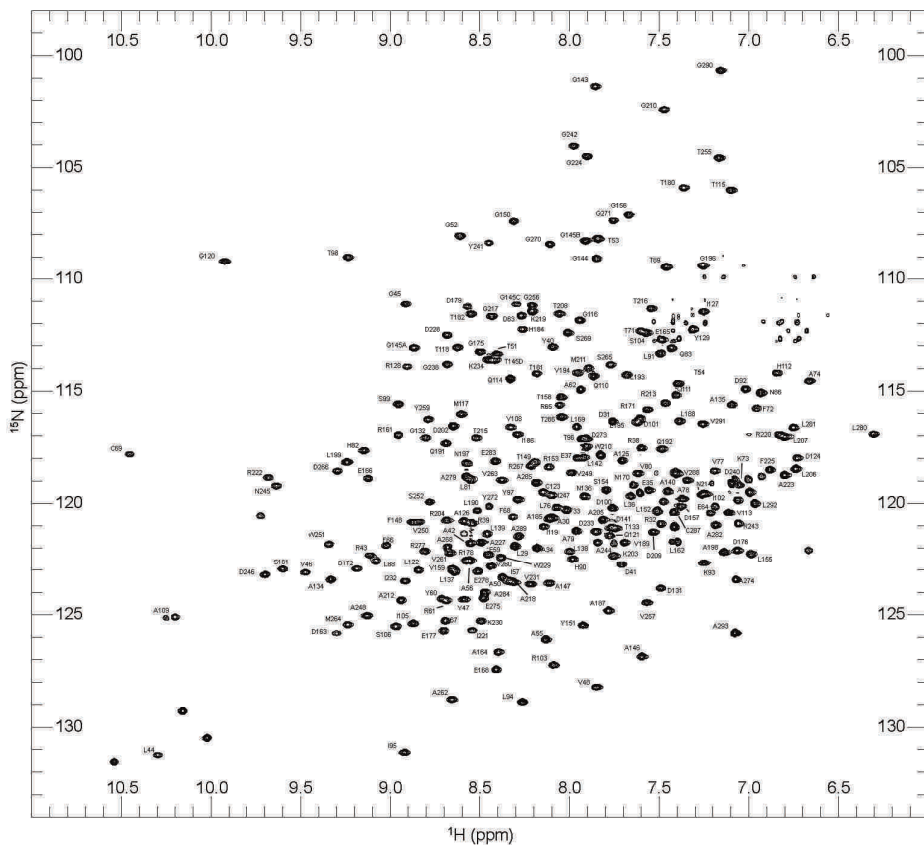


**Figure S2.8.** TROSY-HSQC spectrum of BlaC G269S with residue assignments. Spectrum was obtained at 25 °C using a Bruker AVIII HD 850 MHz spectrometer equipped with a TCI cryoprobe. Sample contained ca. 0.15 mM  $^{15}\text{N}$  BlaC in 100 mM sodium phosphate (pH 6.4) and 6%  $\text{D}_2\text{O}$ . Numbering refers to Ambler numbering.<sup>65</sup> The assignments of the backbone amide resonances have been deposited in the BMRB under entry 50564.

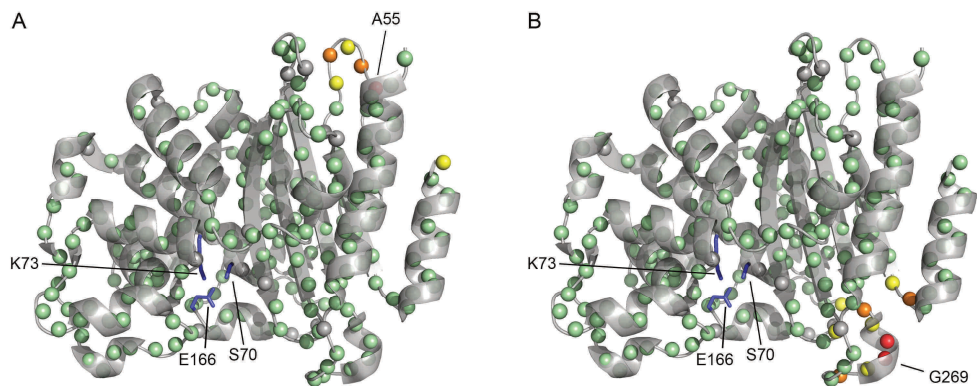


**Figure S2.9.** Average CSP of BlaC A55E (A) and BlaC G269S (B) plotted on the crystal structure of wild-type BlaC (PDB entry 5NJ2<sup>81</sup>). Backbone amides are represented as spheres and those with CSPs greater than 0.025, 0.05, and 0.1 ppm are colored yellow, orange, and red, respectively, those with no or small CSPs are in green, and the ones for which no data were available are colored gray. Mutation sides are indicated and the side chains of active site residues S70, K73 and E166 are represented as sticks. For amides that were detected in the wild-type spectrum, but undetectable in the mutant spectrum, we determined the minimal chemical shift with reference to unassigned peaks and used these values to determine the CSP.

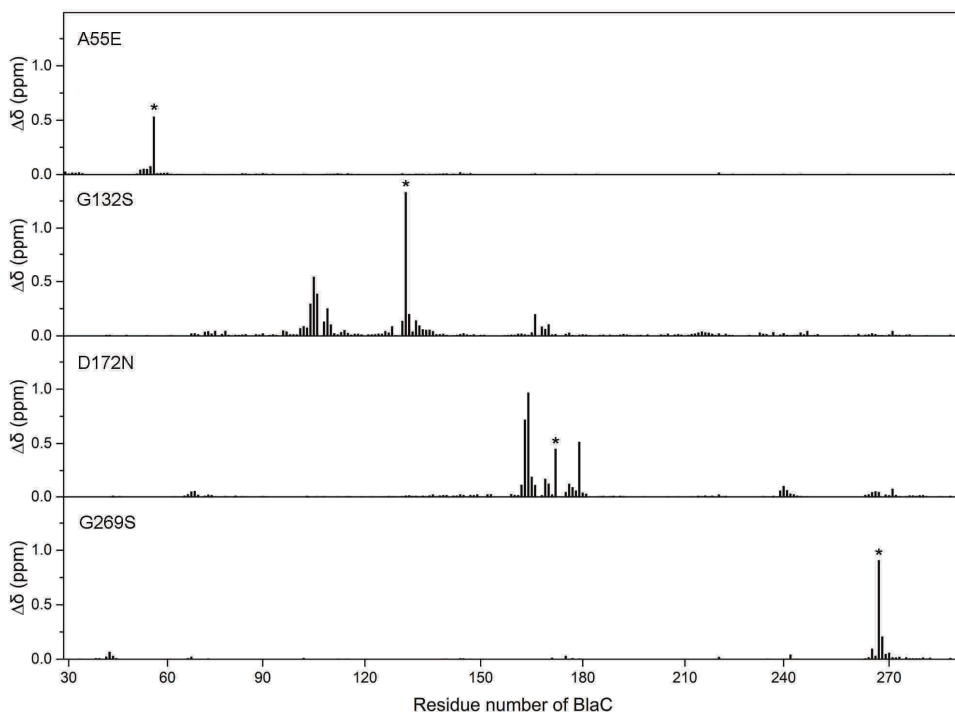


**Figure S2.10.** Average CSP for the backbone amides of the BlaC mutants. Residue numbers refer to Ambler numbering.<sup>65</sup> Mutated residues are indicated with an asterisk.



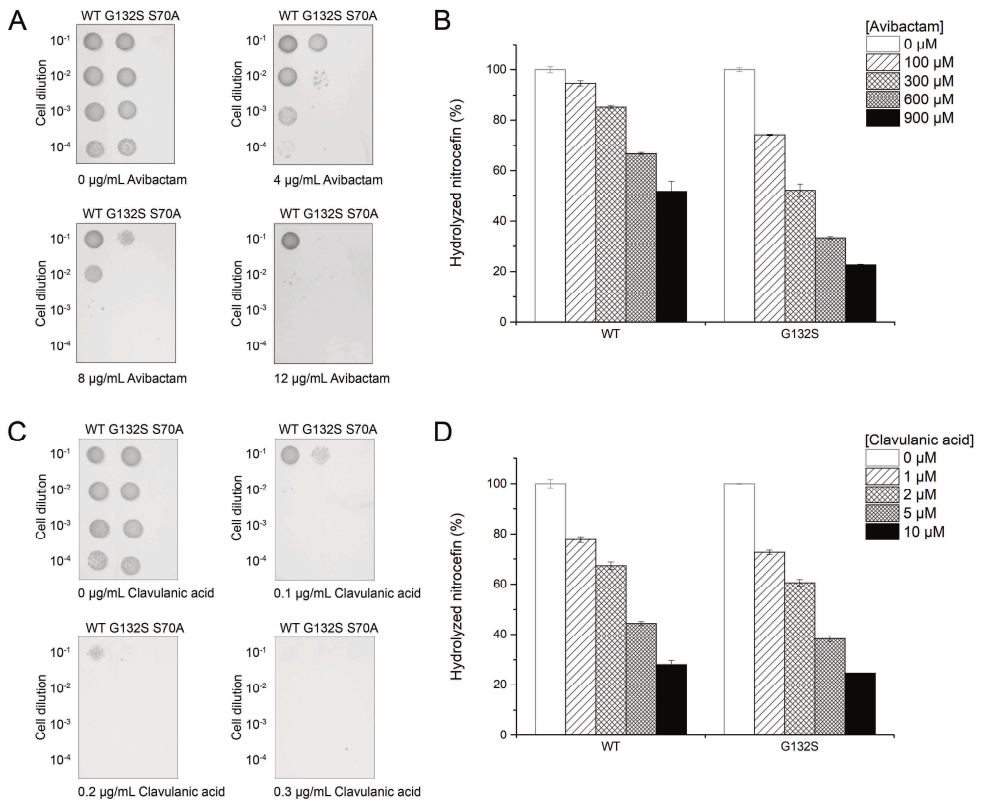


**Figure S2.11.** Activity of Mtb BlaC G132S. (A, C) *E. coli* cells expressing the genes of wild-type BlaC or BlaC G132S were spotted on a plate containing 10 µg mL<sup>-1</sup> ampicillin and (A) avibactam or (C) clavulanic acid. BlaC S70A cannot hydrolyze ampicillin and is used as a negative control. (B, D) Hydrolysis of nitrocefin by wild-type BlaC or BlaC G132S in the presence of avibactam (B) or clavulanic acid (D) for 15 minutes at 25 °C. Measurements were performed in duplicate. The error bars represent one standard deviation.

```

MANNDLFQAS RRRFLAQLGG LTVAGMLGPS LLTPRRATAA 30 40
QADLADRFAE LERRYDARLG

50 60 70 80 90 100
VYVPATGTTA AIEYRADERF AFCSTFKAPL VAAVLHQNPLT HLDKLITYT SDDIRSISPV

110 120 130 140 150 160
AQQHVTGMT IGQLCDAAIR YSDGTAAANLL LADLGGPPGGT AAFTGYLRS LGDTVSRLDA

170 180 190 200 210 220
EPELNRPDP GDERDTTTPH AIALVLQQLV LGNALPPDKRA LLTDWMARN TTGAKRIRAG

230 240 250 260 270 280
FPADWKVIDK TGTGDYGRAN DIAVWVSPTG VPYVVAVMSDR AGGGYDAEP REALLAEAAAT

290
CVAGVLALEH HHHHH

```

**Figure S2.12.** Amino acid residues of BlaC as used for *in vivo* experiments. Residues 28-291 are numbered according to Ambler notation,<sup>65</sup> this corresponds to residue numbers 43-307 of BlaC Uniprot entry P9WKD3-1. Residues of the Tat-signal sequence are underlined, and the His-tag residues are highlighted in gray.

```

MGSSHHHHHH SSGLVPRGSH MENLYFQGDL 30 40 50 60
ADRFAELERR YDARLGVYVP ATGTTAAIEY

70 80 90 100 110 120
RADERFAFCS TFKAPLVAAV LHQNPLTHLD KLITYTSDDI RSISPAQQH VQTGMTIGQL

130 140 150 160 170
CDAAIRYSDG TAANLLLADL GPPGGGTAAF TGYLRS LGDT VSRLDAEEPE LNRDPPGDER

180 190 200 210 220 230
DTTTPHAIAL VLQQLVLGNA LPPDKRALLT DWMARNTTGA KRIRAGFPAD WKVIDKTGTG

240 250 260 270 280 290
DYGRANDIAV VWSPTGVPYV VAVMSDRAGG GYDAEPREAL LAEAATCVAG VLA

```

**Figure S2.13.** Amino acid residues of BlaC as used for *in vitro* experiments. Residues 28-291 are numbered according to Ambler notation,<sup>65</sup> this corresponds to residue numbers 43-307 of BlaC Uniprot entry P9WKD3-1. Residues of the TEV-cleavable His-tag are highlighted in gray.